INDEX COPERNICUS INTERNATIONAL

Bio-Algorithms and Med-Systems

WWW.BAMSJOURNAL.COM ISSN: 1896-530X

ORIGINAL ARTICLE

Received: 07.11.2023
Accepted: 03.12.2023
Published: 31.12.2023

CITE THIS ARTICLE AS:
Kozani MK, Rucinski A, Moskal P, "J-PET application as a Compton camera for proton beam range verification: A preliminary study," BAMS vol. 1, no. 1, pp. 23-30, 2023, DOI: 10.5604/01.3001.0054.1819

AUTHORS' CONTRIBUTION:
A – Study Design
B – Data Collection
C – Statistical Analysis
D – Manuscript Preparation
E – Literature Search
F – Funds Collection

CORRESPONDING AUTHOR:
Majid Kazemi Kozani;
Department of Radiology, University of Pennsylvania, Philadelphia, USA;
E-mail: majid.kazemi@pennmedicine.upenn.edu

J-PET application as a Compton camera for proton beam range verification: A preliminary study

Majid Kazemi Kozani[1,2] (ORCID: 0000-0002-7460-3926), Antoni Rucinski[2] (ORCID: 0000-0002-5815-4606), Pawel Moskal[3] (ORCID: 0000-0002-4229-3548)

[1]Department of Radiology, University of Pennsylvania, Philadelphia, USA
[2]Institute of Nuclear Physics Polish Academy of Sciences, Krakow, Poland
[3]Center for Theranostics, Jagiellonian University, Krakow, Poland

ABSTRACT

Hybrid in-beam PET/Compton camera imaging currently shows a promising approach to use of the quasi-real-time range verification technique in proton therapy. This work aims to assess the capability of utilizing a configuration of the Jagiellonian-positron emission tomography (J-PET) scanner made of plastic scintillator strips, so as to serve as a Compton camera for proton beam range verification. This work reports the production yield results obtained from the GATE/Geant4 simulations, focusing on an energy spectrum (4.2–4.6) MeV of prompt gamma (PG) produced from a clinical proton beam impinging on a water phantom. To investigate the feasibility of J-PET as a Compton camera, a geometrical optimisation was performed. This optimisation was conducted by a point spread function (PSF) study of an isotropic 4.44 MeV gamma source. Realistic statistics of 4.44 MeV PGs obtained from the prior step were employed, simulating interactions with the detector. A sufficient number of detected photons was obtained for the source position reconstruction after performing a geometry optimisation for the proposed J-PET detector. Furthermore, it was demonstrated that more precise calculation of the total deposited energy of coincident events plays a key role in improving the image quality of source distribution determination. A reasonable spatial resolution of 6.5 mm FWHM along the actual proton beam direction was achieved for the first imaging tests. This preliminary study has shown notable potential in using the J-PET application for in-beam PET/Compton camera imaging at quasi-real-time proton range monitoring in future clinical use.

KEYWORDS

proton therapy, prompt gamma, Compton camera, J-PET, range verification

INTRODUCTION

In the past ten years, proton therapy has gained significant importance as a radiotherapy technique, leading to the establishment of dedicated treatment centres around the globe. Its rising popularity can be attributed to the favourable way in which protons deposit energy, featuring a Bragg peak at the end of their path within the patient's tissues [1, 2]. This characteristic ensures precise dose deposition, minimizing damage to healthy tissue, a distinct advantage over traditional photon radiotherapy. However, uncertainties arising from factors such as anatomical changes, patient positioning, and treatment planning necessitate the incorporation of safety margins during irradiation. Implementing an efficient real-time monitoring method for proton therapy can potentially decrease these safety margins, subsequently enhancing the precision of treatment administration [3, 4].

Real-time monitoring of dose distribution in proton therapy may be achieved by detecting the secondary gammas [5, 6], neutrons [7, 8], or positron-emitting substances [9, 10] generated during nuclear reactions of protons with the atomic nuclei of patient tissue.

The most clinical imaging method used for proton range monitoring is positron emission tomography (PET), based on the detection of 511 keV gamma rays resulting from positron emission decay of proton-induced radioactive nuclides such as ^{11}C, ^{13}N, and ^{15}O [10, 11]. Four different PET acquisition protocols, including in-room, off-line, in-beam, and inter-spill modes, are currently performed for proton range monitoring [4]. Nonetheless, the two former approaches face challenges due to the limited efficacy of reconstructed activity images, attributed to the low effective activity within the patient's body and the impact of physiological processes leading to washout effects [12–14]. During the in-beam mode, although the washout effects decrease, a high level of noise is introduced to the registered coincidences due to all secondary particles' contribution [15]. Furthermore, for the last two modes it is not possible to perform full-ring PET scanners due to geometrical limitations. Therefore, unconventional PET configurations have been designed and tested for proton beam range verification [16, 17].

Another promising approach for dose monitoring is the detection of prompt gammas (PGs) emitted in nuclear reactions of protons with the atomic nuclei [18] in tissue. It has been observed that the number of PGs is much larger than the number of positron emissions resulting from PET isotope decay [10]. Furthermore, the absence of washout effects in PG measurement [19] and good correlation between the proton range and PG distribution [20–23] are other important advantages that make measuring PGs a viable method for clinical application.

Various approaches utilizing PG information for real-time proton range monitoring are currently under development, such as PG timing [24–26], gamma-ray spectroscopy [21, 27], and PG imaging. The latter involves the development of two main monitoring systems, a passive approach, e.g. knife-edge-slit cameras [5, 28–30], and an active one, such as Compton cameras [31–33]. Compton cameras generally consist of one or more detection planes, referred to as "scatterer(s)", and a final plane that acts as the "absorber". Using the deposited energies and the interaction positions of PGs interacting via the Compton effect with the detector, the reconstruction of PG emission distribution is feasible. Despite its potential [34–36], a significant obstacle in the realization of real-time Compton camera imaging is the limited signal-to-background ratio observed in clinical settings. This challenge primarily stems from several factors, including the reduced effectiveness of radiation detectors at high gamma-ray -energies [37, 38], restricted detector performance under conditions of high counting rates [2], and the presence of unwanted radiation stemming from scattered protons [39] and neutrons [21, 40].

The idea of hybrid detection modalities was introduced as an alternative strategy to tackle the limitations mentioned earlier [41]. The proposed integration of PET and Compton imaging holds the potential to leverage the enhanced resolution and sensitivity of modern PET technology [42]. Concurrently, it can also address the constraints that PET faces when using multiple radiotracers for molecular imaging [43–45]. Furthermore, recent studies [46] indicate that hybrid PET/Compton camera systems might offer a viable method for quasi-real-time proton range monitoring. This idea relies on the complementary strengths of both methodologies: PG emission holds substantial promise for real-time monitoring, while PET imaging provides valuable tomographic and functional insights that enable the tracking of physiological processes and assessment of tumour response.

In this work, we report on the feasibility of the Jagiellonian PET (J-PET) scanner [47, 48] utilizing plastic scintillator strips as a Compton camera imaging device for proton range verification. To the best of our knowledge, this work represents the first implementation of a plastic scintillator detection system as a Compton camera for high-energy PGs emitted during proton therapy. The performance of the J-PET, with a triple-layer, dual-head design for in-beam range monitoring has been studied in detail in our previous work, on the basis of Monte Carlo simulations [49]. In this study, we conducted Monte Carlo simulations to assess the viability of the proposed J-PET with a modified configuration. Our findings showcase the J-PET's capabilities as a Compton camera and its capacity to tackle the challenges arising from the PET/Compton camera combination for quasi-real-time monitoring of proton beam range.

MATERIALS AND METHODS

J-PET scanner simulations

J-PET technology employs plastic scintillator strips to detect 511 keV coincidence photons through the process of Compton scattering [50]. These strips can be arranged in an axial configuration, enabling a multilayer arrangement [51, 47]. The existing modular design consists of 13 rectangular BC-420 plastic scintillator strips, each

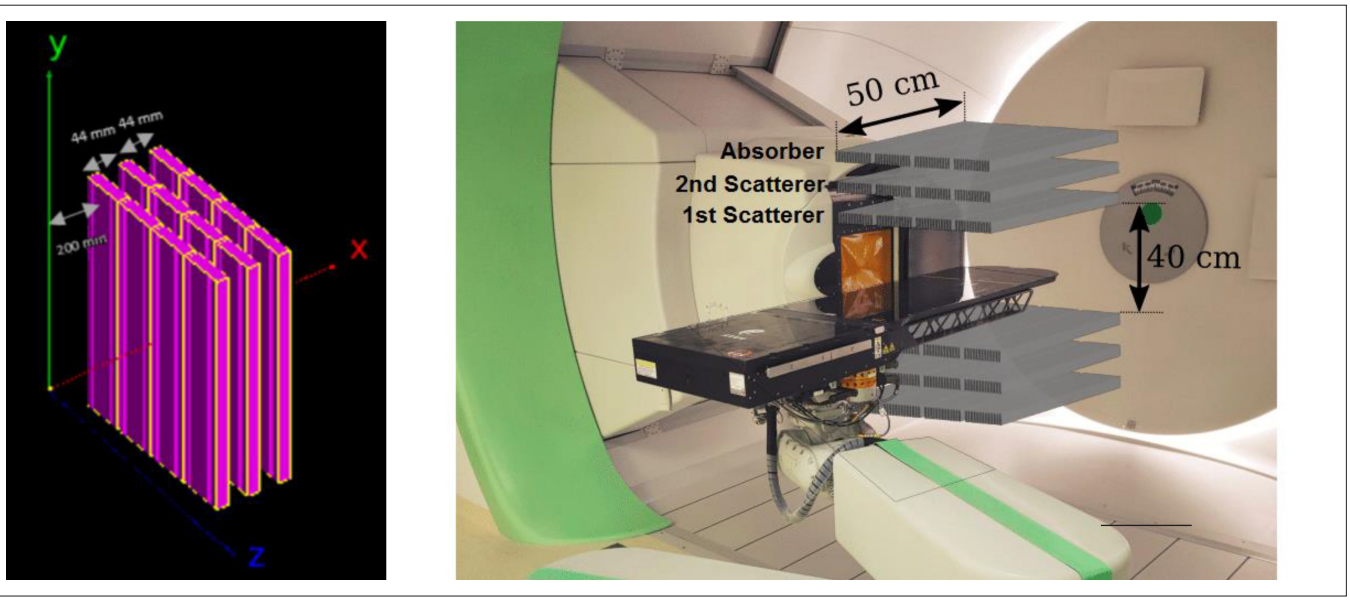

Fig. 1. Left: The simulated one-head geometry and relative distances in the detection setup. Right: The triple-layer, dual-head J-PET for the in-beam protocol. The scatterer and absorber layers are shown in the Compton mode at the starting point of the geometrical optimisation study. Adapted from [49] licensed under CC BY 4.0.

having a volume of 24 × 500 × 6 mm^3. The stack strips are arranged into layers with a pitch of 7 mm in the transverse direction (along the z-axis), which are read out at both ends using silicon photomultipliers (SiPMs). Fig. 1. in the right panel displays the triple-layer dual-head J-PET design proposed for the in-beam protocol. The placement of the scatterers and absorber are also shown for the following geometrical optimisation study at the starting point. Having excellent intrinsic timing properties [50] allowing for electronic collimation, and the flexibility to reconfigure various geometries with the same number of modules, the J-PET scanner could hold significant promise as a Compton camera for proton range monitoring.

To initiate the study, we should explore the performance of a specific J-PET head, such as the top head depicted in Fig. 1. on the left panel, functioning as a Compton camera. Subsequently, the layers of another head can be incorporated into the first, either in a layer-wise manner or by rotating the entire head 180° around the z-axis, positioned realistically with respect to the beam direction in the setup. Therefore, a thorough optimisation of the proposed detector using Monte Carlo simulations is required from the outset. All of the simulation studies in this work were performed with GATE platform version 9.2 [52, 53], based on Geant4 simulation version 11.0.1 [54]. The Compton Camera Module (CCMod) developed by [55] (available in the GATE toolkit) was used to simulate the performance of the J-PET prototype interacting with a point-like isotropic and monoenergetic 4.44 MeV gamma source. To have realistic statistics of 4.44 MeV PGs, a total of 10^8 protons from a 150 MeV clinical beam [56] impinging on a water phantom with a dimension of 50 × 50 × 265 mm^3 was simulated. The predefined QGSP_BIC_HP_EMZ physics list [57] was used to define the physical processes and their corresponding probabilities in the study. Production threshold values were set to 0.1 mm to obtain an optimal balance between achieving an accurate simulation for spatial dose distribution and minimizing computation time [58, 59]. Fig. 2. illustrates the energy spectra of PGs that originate in the water phantom from any physical interactions. The emission of the 4.44 MeV PG line is a result of the de-excitation process of ^{12}C nuclei, which originates from the interactions of protons with ^{16}O nuclei [60]. A production yield per incident proton of 1.81% was achieved by considering an energy window of 4.2–4.6 MeV (shown in Fig. 2.) to estimate the 4.44 MeV PG line contribution and analysing the spatial correlation between its emission and the proton beam range [61]. Therefore, a point-like gamma source emitting 1.81 × 10^6 photons was simulated for achieving the optimal detection setup of J-PET as a Compton camera. Option 4 of the standard electromagnetic physics list, including the Doppler broadening effect, was selected for this study. Moreover, to take into account experimental effects on the imaging resolution, an energy resolution of $\sigma(E)/E = 0.044/\sqrt{E(\text{MeV})}$ measured for a single-strip J-PET prototype [50]) and a position resolution smeared with a Gaussian distribution having full width at half maximum (FWHM) of 5 mm along the length of the scintillator strips (y-axis) [47] were included in the simulation. Therefore, the spatial resolution of the J-PET detector, defined as the FWHM of the point spread function (PSF), represents its capability of determining the source position distribution as a Compton camera. In this work, CCMod has been implemented as a dedicated GATE actor to produce output containing the interaction positions and the corresponding deposited energies within the J-PET modules for all of the hits. Moreover, the interaction type, position, and primary energy of all incoming photons reaching the detector were stored. Singles were obtained by accumulating hits in each detector layer, relying on a priori information about hit positions, sharing the same parent ID, and involving Compton scattering

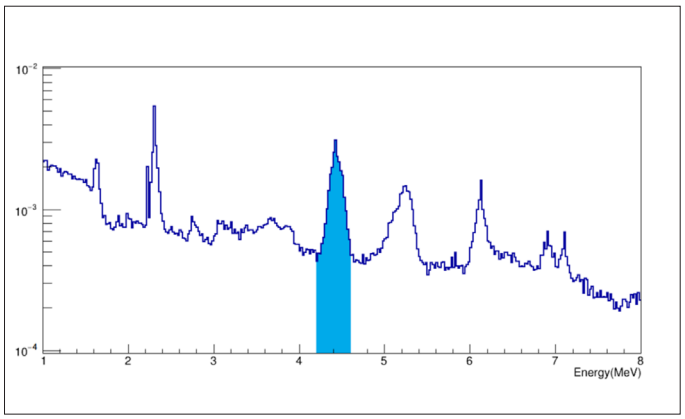

Fig. 2. Energy spectrum of PG generated by a 150 MeV proton beam in water. The area shown in blue was used to estimate the 4.44 MeV PG contribution percentage produced by the proton beam.

interactions. Events with singles having the same parent ID and at least one interaction in both the scatterer and absorber layers were identified as coincident events. Later, the interaction sequences of each coincident event were sorted in chronological order by single time stamp values.

Source position reconstruction

The simulated data was subsequently converted into a desirable format for reconstruction with the use of a list-mode maximum--likelihood expectation maximization (LM-MLEM) algorithm, as described in [62]. In this study, the information on interaction positions and the corresponding deposited energies in each scatterer layer and in the absorber for events having up to three interactions in total were analysed for image reconstruction purposes. As the total deposited energy of most events with two interactions is not collected completely in the detector, this may lead to a deterioration in the source position determination. However, in the case of events with three interactions, the primary energy of the gamma (E_0) can be accurately calculated using the equation [63]

$$E_0 = E_1 + \frac{1}{2}\left(E_2 + \sqrt{E_2^2 + \frac{4E_2 m_e c^2}{1 - \cos\theta_2}}\right), \quad (1)$$

in which E_1 and E_2 are the energy depositions within each scatterer layer, m_e is the electron mass at rest, c is the speed of light, and θ_2 is the second scattering angle. Subsequently, the first scattering angle θ_1 can be calculated using the Compton scattering equation

$$\cos\theta_1 = 1 - m_e c^2 \left(\frac{1}{E_0 - E_1} - \frac{1}{E_0}\right). \quad (2)$$

it should be noted that for each coincident event, the Compton cone's axis is formed by the first two Compton scattering positions, its aperture angle is θ_1 and its apex is the first interaction in each scatterer layer.

Influence of the J-PET geometry on its performance

Due to the low atomic number of plastic scintillators used in the J-PET, a reduced detection efficiency of the coincident events is expected, particularly for PGs at higher energy levels. Therefore, the influence of some geometrical parameters was studied to improve the detection efficiency, finding the optimal geometrical layout in the following sections. The definitions of the detection efficiency (D_E) and true efficiency (T_E) metrics used to evaluate the J-PET response are as follows

$$D_E = \frac{N_c}{N_i}. \quad (3)$$

where N_i is the total number of photons isotropically emitted in $4\pi sr$, and N_c is the total number of events interacting via the Compton effect at the first interaction and with at least one interaction of the scattered photon in another layer of the detector. The category of the events includes true Compton, back-scattering, and randomly scattered events.

$$T_E = \frac{N_t}{N_i}. \quad (4)$$

in which N_t refers to the true Compton events, i.e. corresponding to events whose interaction sequences occur in a forward direction (layer-wise along the x-axis) and having at least one interaction in the final layer (absorber). Taking into account the minimal possible distance from the patient, the source-scatterer distance was fixed at 200 mm for all the presented results.

RESULTS

Influence of the inter-detector distances

Fig. 3. presents the detection efficiency dependence as a function of the inter-detector distances for one head of the J-PET. It can be seen that D_E and T_E increase by a significant factor of 4.2 and 4.6 when the inter-detector distances decrease from 10 to 1 cm, respectively. As expected, the solid angle subtended by each layer of the detector at the previous one increases when the inter-detector distances decrease, leading to a significant increase in the efficiency values.

Influence of the number of layers in the scatterer

The number of layers (n) in the scatterer was changed while keeping the inter-detector distances at 1 cm. As depicted, the detection efficiency improves when the number of scatterer layers increases from 2 to 5, due to a two-fold increase in the contribution of true Compton events (see Fig. 4.). Thus, considering five layers as the scatterers and the final one as the absorber provides relatively sufficient statistics for true Compton events (~10^3 coincidences

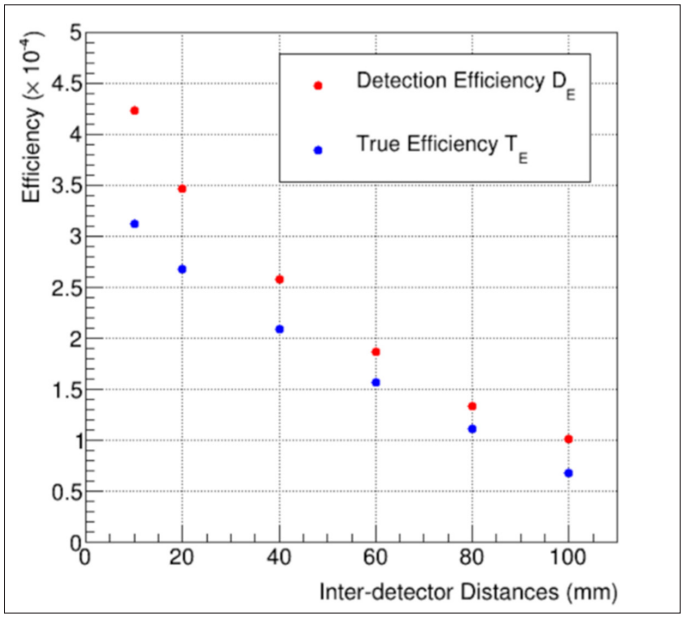

Fig. 3. Influence of inter-detector distances on D_E and T_E.

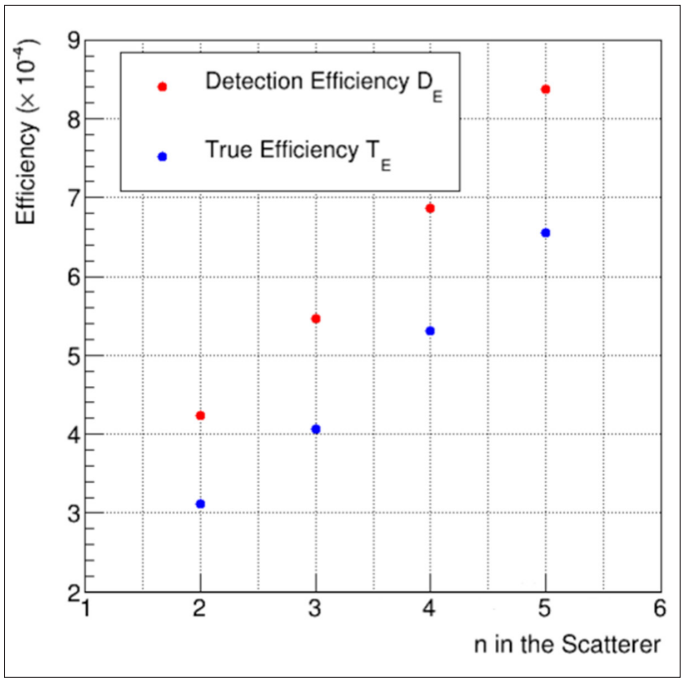

Fig. 4. Influence of n in the scatterer on D_E and T_E.

Tab. I. Number of true Compton and background events for the J-PET's final configuration.

NUMBER OF INTERACTIONS	TRUE COMPTON	BACKGROUND	TOTAL EVENTS
2	708	214	922
3	477	118	595

for a single proton beam spot (~10^8) in clinical use [32]) for the source position reconstruction (see Tab. I.).

As is shown, a total number of 1.52×10^3 coincident events were detected in the proposed J-PET, in which 61% and 39% belong to events with two and three interactions in total, respectively.

Image reconstruction assessment

As previously mentioned in section 2, the quality of reconstructed images obtained from the PSF study could be an evaluation metric for J-PET performance as a Compton camera and allow for further geometrical optimisation. The 2D profiles of the point source were reconstructed. For all the presented results, a pixel-wise convergence criterion was implemented in the LM-MLEM algorithm [64]. Fig. 5. displays the fitting result of the PSF, showing spatial resolutions of 11 mm and 20 mm FWHM along the z- and y-axes, respectively. This refers to the higher contribution of events with two interactions in the image reconstruction, leading to a broader activity distribution in both directions. This could be challenging when taking such events into account in the image reconstruction stage.

Fig. 6. shows that image reconstruction using only the information concerning events with three interactions. Although the image quality along the y-axis is still not informative, it displays a superior determination of the source position along the z-axis (the proton beam direction in the real clinical setting), with a spatial resolution of 6.5 mm FWHM. This illustrates that the more accurate the total deposited energy of detected events within the detector, the more precise the reconstructed source position distribution, in spite of the limited number of such events resulting in white pixels in the 2D reconstructed profile after a few number of LM--MLEM iterations. Therefore, correcting the deposited energy of events with two interactions, either using the machine learning approaches proposed by [33, 38] or by optimising the geometry and evaluating its performance through more detailed Monte Carlo simulations and measurements, could significantly improve the source position determination.

DISCUSSION

The primary objective of this study was to utilize Monte Carlo simulations to investigate the feasibility of the J-PET as a Compton imaging device for verifying the range of proton beams. To achieve this goal, a series of GATE simulations were performed to analyse the capability of the J-PET application in the context of the Compton camera imaging system. Firstly, the simulation involved a clinical 150 MeV proton beam interacting with a water phantom, estimating the PG emissions production yield. Later, the interaction of the number of photons obtained from the initial study (1.81×10^6) with an energy of 4.44 MeV and one head of the J-PET detector was simulated to optimise its geometrical configuration.

It was shown that besides decreasing the inter-detector distances, increasing the number of scatterer layers up to 5 results in a satisfactory number of coincident events for the presented

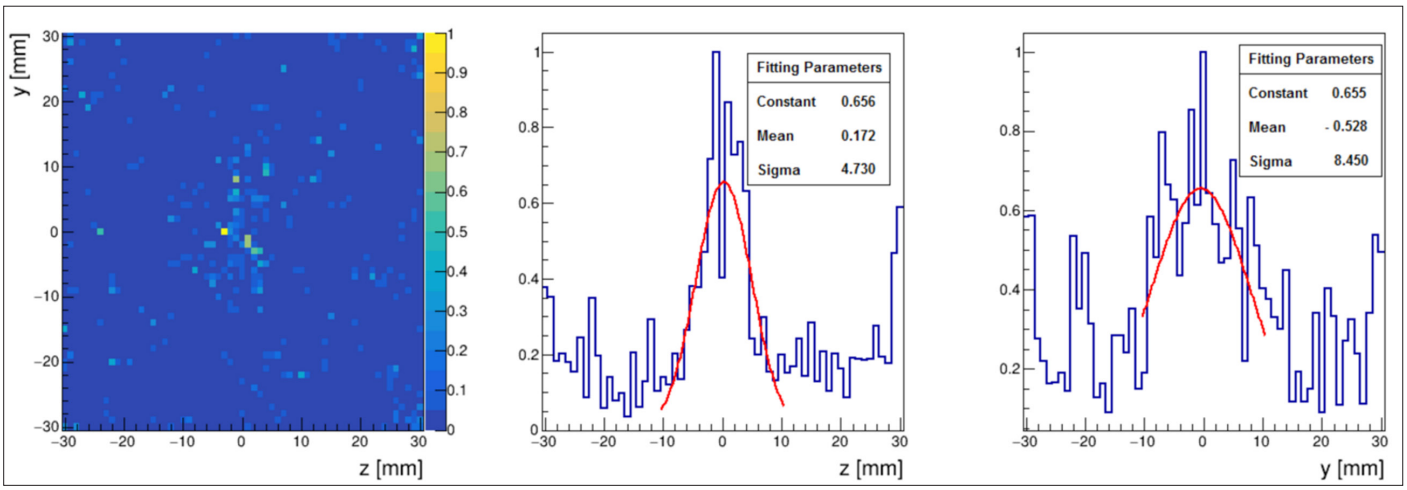

Fig. 5. Reconstructed image of the 4.44 MeV point source located at (0,0) using all events (left), 1D profile along the z-axis (middle), and transverse line profile along the y-axis (right). The reconstructed image was obtained after reaching convergence. All profiles were normalized by their maximum intensity value.

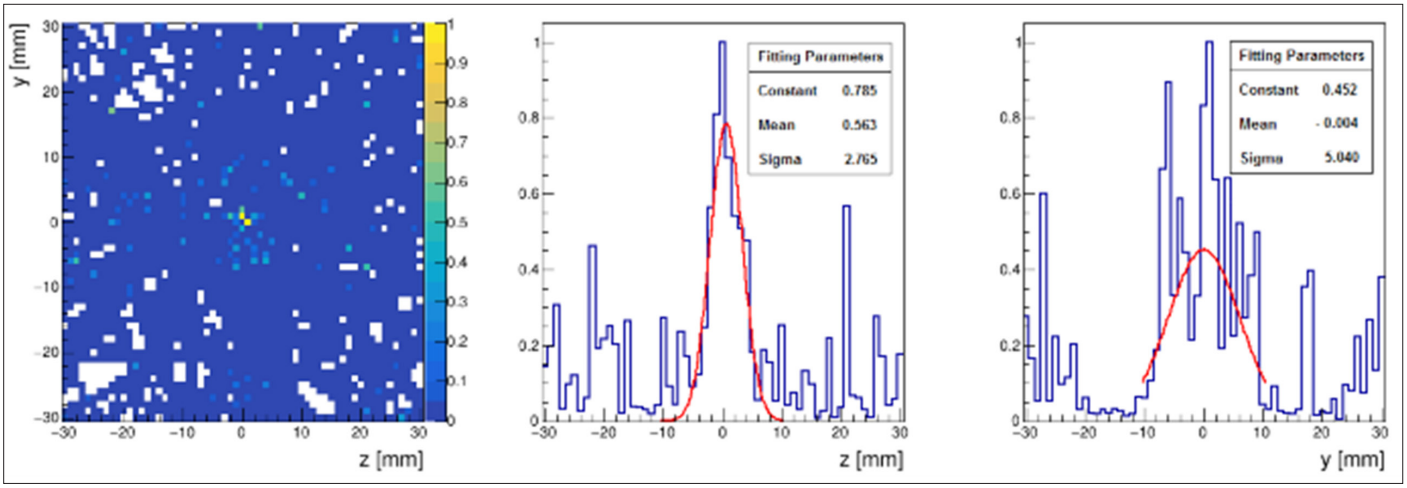

Fig. 6. 2D Reconstructed image of the 4.44 MeV point source located at (0,0) using events with three interactions (left), 1D profile along the z-axis (middle), and 1D profile along the y-axis (right). The reconstructed image was obtained after reaching convergence. All profiles were normalized by their maximum intensity value.

PSF study. While the optimisation of the J-PET's geometry yielded a notable enhancement of approximately one order of magnitude (~ 9.7) in true efficiency, the utilization of information from all detected coincident events did not lead to a reasonable spatial resolution for the position of the point source. The main reason is due to a lack of information on the total deposited energy of events having two interactions. However, it was shown that reconstructing the source position using only events with three interactions yielded a satisfactory spatial resolution of 6.5 mm FWHM along the z-axis, despite the limited number of such events. Consequently, a more sophisticated approach is required when it comes to including events with two interactions, such as machine-learning methods for recovering energy deposition, thus obtaining the reconstructed source position more accurately at the end.

CONCLUSIONS

A preliminary study of the J-PET prototype optimisation was performed, utilizing a Compton camera for reconstructing the source position distribution. This proposed J-PET configuration demonstrates considerable potential for quasi-real-time proton beam range monitoring as a hybrid in-beam PET/Compton in future clinical applications.

ACKNOWLEDGEMENTS

We gratefully acknowledge the support provided by the Foundation for Polish Science through the TEAM POIR.04.04.00-00-4204/17 program.

REFERENCES

1. Wilson RR. Radiological use of fast protons. Radiology. 1946;47:487-91.
2. Knopf AC, Lomax A. In vivo proton range verification: a review. Phys Med Biol. 2013;58:R131-60.
3. Paganetti H. Range uncertainties in proton therapy and the role of Monte Carlo simulations. Phys Med Biol. 2012;57:99-117.
4. Kraan AC. Range verification methods in particle therapy: Underlying physics and Monte Carlo modeling. Front Oncol. 2015;5:150.
5. Kim JW. Pinhole camera measurements of prompt gamma-rays for detection of beam range variation in proton therapy. J Kor Phys Soc. 2009;55:1673-76.
6. Krimmer J, Dauvergne D, Letang J, Testa E. Prompt-gamma monitoring in hadrontherapy: A review. Nucl Instrum Methods Phys Res Sect A: Acceler Spectrom Detect Assoc Equip. 2018;878:58-73.
7. Marafini M, Gasparini L, Mirabelli R, Pinci D, Patera V, Sciubba A, et al. Mondo: a neutron tracker for particle therapy secondary emission characterisation. Phys Med Biol. 2017;62:3299.
8. Ytre-Hauge KS, Skjerdal K, Mattingly J. A Monte Carlo feasibility study for neutron based real-time range verification in proton therapy. Sci Rep. 2019;9:2011.
9. Enghardt W, Crespo P, Fiedler F, Hinz R, Parodi K, Pawelke J, et al. Charged hadron tumour therapy monitoring by means of PET. NIM A. 2004;525:284-8.
10. Moteabbed M, Espana S, Paganetti H. Monte Carlo patient study on the comparison of prompt gamma and PET imaging for range verification in proton therapy. Phys Med Biol. 2011;56:1063-82.
11. Parodi K, Yamaya T, Moskal P. Experience and new prospects of PET imaging for ion beam therapy monitoring. Z Med Phys. 2023;33:22-34.
12. Parodi K, Paganetti H, Shih HA, Michaud S, Loeffler JS, Thomas F, et al. Patient study of in vivo verification of beam delivery and range, using positron emission tomography imaging after proton therapy. Nucl Instrum Methods Phys Res Sect A. 2007;68:920-34.
13. Knopf AC, Parodi K, Paganetti H, Bortfeld T, Daartz J, Engelsman M, et al. Accuracy of proton beam range verification using post treatment positron emission tomography/computed tomography as function of treatment site. Int J Radiat Oncol Biol Phys. 2011;79:297-304.
14. Min CH, Zhu X, Winey BA, Grogg K, Testa M, El Fakhri G, et al. Clinical application of in-room positron emission tomography for in vivo treatment monitoring in proton radiation therapy. Int J Radiat Oncol Biol Phys. 2013;13:183-9.
15. Fiedler F, Shakirin G, Skowron J, Braess H, Crespo P, Kunath D, et al. On the effectiveness of ion range determination from in-beam PET data. Radiology. 2010;55:1989-98.
16. Ferrero V, Fiorina E, Morrocchi M, Pennazio F, Baroni G, Battistoni G, et al. Online proton therapy monitoring: clinical test of a Siliconphotodetector-based in-beam PET. Sci Rep. 2018;8:4100.
17. Fiorina E, Ferrero V, Baroni G, Battistoni G, Belcari N, Camarlinghi N, et al. Detection of inter-fractional morphological changes in proton therapy: a simulation and in-vivo study with the INSIDE in-beam PET. Front Phys. 2020;8:660.
18. Bom V, Joulaeizadeh L, Beekman F. Real-time prompt gamma monitoring in spot-scanning proton therapy using imaging through a knife-edge-shaped slit. Phys Med Biol. 2012;57:297-308.
19. Knopf A, Parodi K, Bortfeld T, Shih HA, Paganetti H. Systematic analysis of biological and physical limitations of proton beam range verification with offline PET/CT scans. Phys Med Biol. 2009;54:4477-95.
20. Min CH, Kim CH, Youn MY, Kim JW. Prompt gamma measurements for locating the dose falloff region in the proton therapy. Appl Phys Lett. 2006;89:183517.
21. Verburg JM, Seco J. Proton range verification through prompt gamma-ray spectroscopy. Phys Med Biol. 2014;59:7089-106.
22. Pinto M, Bajard M, Bronset S, Chevallier M, Dauvergne D, Dedes G, et al. Absolute prompt-gamma yield measurements for ion beam therapy monitoring. Phys Med Biol. 2015;60:565-94.
23. Kelleter L, Wronska A, Besuglow J, Konefa A, Laihem K, Leidner J, et al. Spectroscopic study of prompt-gamma emission for range verification in proton therapy. Phys Med. 2017;34:7-17.
24. Golnik C, Hueso-Gonzalez F, Muller A, Dendooven P, Enghardt W, Fiedler F, et al. Range assessment in particle therapy based on prompt γ-ray timing measurements. Phys Med Biol. 2014;59:5399-422.
25. Hueso-Gonzalez F, Enghardt W, Fiedler F, Golnik C, Janssens G, Petzoldt J, et al. First test of the prompt gamma ray timing method with heterogeneous targets at a clinical proton therapy facility. Phys Med Biol. 2015;60:6247-72.
26. Krimmer J, Angellier G, Balleyguier L, Dauvergne D, Freud N, Herault J, et al. A cost-effective monitoring technique in particle therapy via uncollimated prompt gamma peak integration. Appl Phys Lett. 2017;110:154102.
27. Hueso-Gonzalez F, Rabe M, Ruggieri TA, Bortfeld T, Verburg JM. A full-scale clinical prototype for proton range verification using prompt gamma-ray spectroscopy. Phys Med Biol. 2018;63:185019.
28. Kim CH, Park JH, Seo H, Lee RL. Gamma electron vertex imaging and application to beam range verification in proton therapy. Med Phys. 2012;39:1001-5.
29. Verburg JM, Riley K, Bortfeld T, Seco J. Energy- and time-resolved detection of prompt gamma-rays for proton range verification. Phys Med Biol. 2013;58:L37-L49.
30. Jan ML, Hsiao IT, Huang HM. Use of a LYSO-based Compton camera for prompt gamma range verification in proton therapy. Med Phys. 2017;44:6261-9.
31. Peterson SW, Robertson D, Polf JC. Optimizing a three-stage Compton camera for measuring prompt gamma rays emitted during proton radiotherapy. Phys Med Biol. 2010;55:6841-56.
32. Kasper J, Rusiecka K, Hetzel R, Kazemi KM, Lalik R, Magiera A, et al. The SiFi-CC project - Feasibility study of a scintillation fiber-based Compton camera for proton therapy monitoring. Phys Med. 2020;76:317-25.
33. Munoz E, Ros A, Borja-Lloret M, Barrio J, Dendooven P, Oliver JF, et al. Proton range verification with MACACO II Compton camera enhanced by a neural network for event selection. Sci Rep. 2021;11:9325.
34. Gillam J, Lacasta C, Torres-Espallardo I, Candela-Juan C, Llosa G, Solevi P, et al. A Compton imaging algorithm for on-line monitoring in hadron therapy. Phys Med Imaging. 2011;7961:79611O.
35. Draeger E, Mackin D, Peterson S, Chen H, Avery S, Beddar S, et al. 3D prompt gamma imaging for proton beam range verification. Phys Med Biol. 2018;63:035019.
36. Munoz E, Barrientos L, Bernabeu J, Borja-Lloret M, Llosa G, Ros A, et al. A spectral reconstruction algorithm for two-plane Compton cameras., Phys Med Biol. 2020;65:025011.
37. Polf JC, Avery S, Mackin DS, Beddar S. Imaging of prompt gamma rays emitted during delivery of clinical proton beams with a Compton camera: Feasibility studies for range verification. Phys Med Biol. 2015;60:7085-99.
38. Kazemi KM, Magiera A. Machine learning-based event recognition in SiFi Compton camera imaging for proton therapy monitoring. Phys Med Biol. 2022;67:155012.
39. Ortega PG, Torres-Espallardo I, Cerutti F, Ferrari A, Gillam JE, Lacasta C, et al. Noise evaluation of Compton camera imaging for proton therapy. Phys Med Biol. 2015;60:1845-63.
40. Polf JC, Parodi K. Imaging particle beams for cancer treatment. Phys Today. 2015;68:28-33.

41. Parodi K. On- and off-line monitoring of ion beam treatment. Nucl Inst Methods Phys Res A. 2016;809:113-9.
42. Shimazoe K, Uenomachi M. Multi-molecule imaging and inter-molecular imaging in nuclear medicine. Bio-Algorithms and Med-Systems (BAMS). 2022;18:127-34.
43. Yoshida E, Tashima H, Nagatsu K, Tsuji A, Kamada K, Parodi K, et al. Whole gamma imaging: a new concept of PET combined with Compton imaging. Phys Med Biol. 2020;65:125013.
44. Uenomachi M, Shimazoe K, Takahashi H. A double photon coincidence detection method for medical gamma-ray imaging. Bio-Algorithms and Med-Systems (BAMS). 2022;18:120-6.
45. Llosa G, Rafecas M. Hybrid PET/Compton-camera imaging: an imager for the next generation. Eur Phys J Plus. 2023;138:214.
46. Balibrea-Correa J, Lerendegui-Marco J, Ladarescu I, Guerrero C, Rodrıguez-Gonzalez T, Jimenez-Ramos MC, et al. Hybrid in-beam PET- and Compton prompt-gamma imaging aimed at enhanced proton-range verification. Eur Phys J Plus. 2023;137:1258.
47. Moskal P, Kowalski P, Shopa RY, Raczynski L, Baran J, Chug N, et al. Simulating NEMA characteristics of the modular total-body J-PET scanner—an economic total-body PET from plastic scintillators. Phys Med Biol. 2021;66:175015.
48. Moskal P, Dulski K, Chug N, Curceanu C, Czerwinski E, Dadgar M, et. al. Positronium imaging with the novel multiphoton PET scanner. Sci Adv. 2021;7:eabh4394.
49. Brzezinski K, Baran J, Borys D, Gajewski J, Chug N, Coussat A, et al. Detection of range shifts in proton beam therapy using the J-PET scanner: a patient simulation study. Phys Med Biol. 2023;68:145016.
50. Moskal P, Niedzwiecki S, Bednarski T, Czerwinski E, Kubicz E, Moskal I, et al. Test of a single module of the J-PET scanner based on plastic scintillators. Nucl Instrum Methods Phys Res A. 2014;764:317-21.
51. Moskal P, Rundel O, Alfs D, Bednarski T, Bia las P, Czerwinski E, et al. Time resolution of the plastic scintillator strips with matrix photomultiplier readout for J-PET tomograph. Phys Med Biol. 2016;61:2025.
52. Jan S, Benoit D, Becheva E, Carlier T, Cassol F, Descourt P, et al. GATE V6: a major enhancement of the GATE simulation platform enabling modelling of CT and radiotherapy. Phys Med Biol. 2011;56:881-901.
53. Sarrut D, Bardiès M, Boussion N, Freud N, Jan S, Létang JM, et al. A review of the use and potential of the gate Monte Carlo simulation code for radiation therapy and dosimetry applications. Med Phys. 2014;41:064301.
54. Agostinelli S, Allison J, Amako K, Apostolakis J, Araujo H, Arce P, et. al. Geant4 — A simulation toolkit. Nucl Instrum Methods Phys Res B NUCL INSTRUM METH A. 2003;506:250-303.
55. Etxebeste A, Dauvergne D, Fontana M, Letang JM, Llosa G, Munoz E, et al. CCMod: a GATE module for Compton Camera imaging simulation. Phys Med Biol. 2020;65:055004.
56. Gajewski J, Garbacz M, Chang CW, Czerska K, Durante M, Krah N, et al. Commissioning of GPU-accelerated Monte Carlo code Fred for clinical applications in proton therapy. Front Phys. 2021;8:567300.
57. Geant4 collaboration. Guide for Physics Lists. Release 10.4. 2020.
58. Zahra N, Frisson T, Grevillot L, Lautesse P, Sarrut D. Influence of Geant4 parameters on dose distribution and computation time for carbon ion therapy simulation. Phys Med. 2010;26:202-8.
59. Kazemi M, Afarideh H, Riazi Z. Evaluation of Open MPI and MPICH2 performances for the Computation Time in Proton Therapy Dose Calculations with Geant4". J Korean Phys Soc. 2015;67:1686-91.
60. Foley KJ, Clegg AB, Salmon GL. Gamma radiation from bombardment of 16O and 19F nuclei with 150 MeV protons. Nucl Phys. 1962;31:43-52.
61. Zarifi M, Guatelli S, Bolst D, Hutton B, Rosenfeld A, Qi Y. Characterization of prompt gamma-ray emission with respect to the Bragg peak for proton beam range verification: A Monte Carlo study. Phys Med. 2016;33:197-206.
62. Wilderman SJ, Clinthorne NH, Fessler JA, Rogers WL. List-mode maximum likelihood reconstruction of Compton scatter camera images in nuclear medicine. EEE Nucl Sci Symp Med Imaging Conf Rec. 1998;3:1716-20.
63. Mackin D, Peterson S, Beddar S, Polf J. Evaluation of a stochastic reconstruction algorithm for use in Compton camera imaging and beam range verification from secondary gamma emission during proton therapy. Phys Med Biol. 2012;57:3537-53.
64. Kohlhase N, Wegener T, Schaar M, Bolke A, Etxebeste A, Sarrut D, et al. Capability of MLEM and OE to detect range shifts with a Compton camera in particle therapy. IEEE Trans Rad and Plasma Med Sci. 2019;4:233-42.